Original article

Nuclear Medicine Communications

Appropriate parameters of the ordered-subset expectation maximization algorithm on measurement of myocardial blood flow and oxygen consumption with ^{11}C-acetate PET

Masato Kobayashi[a,b], Tetsuya Mori[a], Yasushi Kiyono[a], Tetsuya Tsujikawa[a], Rikiya Maruyama[a], Yusuke Higaki[b], Naoto Shikano[c], Ryuichi Nishii[d], Keiichi Kawai[a,b], Takashi Kudo[a,e] and Hidehiko Okazawa[a]

Objective **The purpose of this study was to evaluate the appropriate parameters of a filter and of subsets (S) and iterations (I) of the ordered-subset expectation maximization (OSEM) algorithm in ^{11}C-acetate PET.**

Methods **A Hanning filter (HF) and a Gaussian filter (GF) were selected for filtered back-projection (FBP) and the OSEM algorithm, respectively. After evaluation of the optimal HF size, the GF size was optimized using healthy volunteers (HV). Myocardial blood flow (MBF) and oxygen consumption (k_{mono}) values were calculated by combining 4S, 16S, or 28S with 2I, 4I, 6I, or 8I of the OSEM (MBF_{OSEM} and $k_{monoOSEM}$, respectively) in eight HV and eight coronary artery disease (CAD) patients. These MBF_{OSEM} and $k_{monoOSEM}$ values were compared with those obtained using FBP (MBF_{FBP} and $k_{monoFBP}$, respectively).**

Results **Optimal HF and GF (10.0GF) sizes for the FBP and OSEM algorithms, respectively, were 10.0 mm full-width resolution at half-maximum. MBF_{OSEM} was changed by modifying the parameters of the OSEM algorithm. The best correlations were between MBF_{FBP} and MBF_{OSEM}, with 28S6I and 10.0GF for HV patients and 28S8I for CAD patients. However, the MBF_{OSEM} with 28S8I was significantly different from MBF_{FBP} at the global myocardium in HV. The $k_{monoOSEM}$ with 28S6I was not significantly different from $k_{monoFBP}$ in HV or CAD patients.**

Conclusion **Appropriate parameters are 28S6I with a 10.0GF on the MBF_{OSEM} and $k_{monoOSEM}$ measurement using ^{11}C-acetate. Diagnostic performance will improve using noiseless, artifact-reduction images, and accurate quantitative values that are provided by the OSEM algorithm with the appropriate parameters.** ***Nucl Med Commun*** **33:130–138 © 2012 Wolters Kluwer Health | Lippincott Williams & Wilkins.**

Nuclear Medicine Communications 2012, **33**:130–138

Keywords: ^{11}C-acetate PET, cardiology, myocardial blood flow, myocardial oxygen consumption, ordered-subset expectation maximization

[a]Biomedical Imaging Research Center, University of Fukui, Fukui, [b]School of Health Sciences, College of Medical, Pharmaceutical and Health Sciences, Kanazawa University, Kanazawa, [c]Department of Radiological Sciences, Ibaraki Prefectural University of Health Sciences, Ibaraki, [d]Department of Radiology, School of Medicine, Miyazaki University, Miyazaki and [e]Atomic Bomb Disease Institute, Nagasaki University, Nagasaki, Japan

Correspondence to Masato Kobayashi, PhD, School of Health Sciences, College of Medical, Pharmaceutical and Health Sciences, Kanazawa University, 5-11-80 Kodatsuno, Kanazawa 920-0942, Japan
Tel: +81 76 265 2531; fax: +81 76 234 4351;
e-mail: kobayasi@mhs.mp.kanazawa-u.ac.jp

Received 3 August 2011 **Revised** 19 October 2011 **Accepted** 24 October 2011

Introduction

Image reconstruction processing is an essential step to obtain high image quality in PET. Reconstruction algorithms usually fall into one of two main categories: analytic image reconstruction methods, such as the filtered back-projection (FBP) algorithm, and iterative image reconstruction methods, such as the ordered-subset expectation maximization (OSEM) algorithm [1]. The FBP algorithm is generally used as the gold standard for quantitative PET, whereas the OSEM algorithm improves the image signal-to-noise ratio and eliminates streak artifacts in the PET images because of its more optimal handling of Poisson's noise in the sinogram data.

In cardiac PET studies, the OSEM algorithm yielded accurate quantitative data and improved image quality in comparison with the FBP algorithm when used for measurement of the glucose metabolic rate in ^{18}F-2-fluoro-2-deoxy-D-glucose (^{18}F-FDG) PET [2–4] and for measurement of myocardial blood flow (MBF) in ^{15}N-ammonia PET [4–6]. However, the OSEM algorithm has not been applied to the measurement of MBF [7–12] or oxygen consumption (k_{mono}) [13–22] in ^{11}C-acetate PET. In this study, we evaluated the parameters of an OSEM algorithm, including optimization of a smoothing Gaussian post-filter, which were appropriate for MBF and k_{mono} measurements in ^{11}C-acetate PET. The values of MBF and k_{mono} calculated using OSEM with different parameters were compared with those calculated using FBP in PET studies of healthy volunteers (HV) and coronary artery disease (CAD) patients.

Methods

Participants

Sixteen participants, eight young male HV (age range: 21–36 years; mean: 28.9 ± 6.2 years) and eight CAD

0143-3636 © 2012 Wolters Kluwer Health | Lippincott Williams & Wilkins DOI: 10.1097/MNM.0b013e32834e7f5c

patients with known myocardial ischemia (four men, four women; age range: 60–87 years; mean: 73.0 ± 10.3 years), were studied. All patients fasted for more than 6 h before PET examination. The study was approved by the Ethics Committee of Fukui University Hospital and the experiments have therefore been performed in accordance with the ethical standards laid down in the 1964 Declaration of Helsinki. Written informed consent was obtained from each participant.

Positron emission tomography procedures

All participants underwent PET scanning using a whole-body tomography scanner (ADVANCE, General Electric Medical System, Milwaukee, Wisconsin, USA), which allowed the simultaneous acquisition of 35 image slices in a two-dimensional (2D) acquisition mode with an interslice spacing of 4.25 mm [23]. Performance tests showed the intrinsic resolution of the scanner to be 4.6–5.7 mm in the transaxial direction and 4.0–5.3 mm in the axial direction. A 10 min transmission scan was performed using ^{68}Ge/^{68}Ga for attenuation correction before radiotracer administration. Approximately 740 MBq of ^{11}C-acetate was slowly administered intravenously over 30 s and dynamic data were acquired (5-s × 18 frame, 7-s × 30 frame, 60-s × 5 frame, and 120-s × 5 frame). Transaxial slices were collected in a matrix size of 128 × 128 pixels.

Image processing

A Hanning filter (HF) and a Gaussian filter (GF) were selected as smoothing filters for the FBP and OSEM algorithms, respectively. The projection data were reconstructed using the FBP algorithm with the HF, and the OSEM algorithm, which was combined with several different subset (S) and iteration (I) numbers, with a full-width resolution at half-maximum (FWHM) GF in the transaxial direction. To optimize these filters, the size of the HF was changed to 4.5, 6.0, 8.0, 10.0, or 15.0 mm FWHM (4.5HF, 6.0HF, 8.0HF, 10.0HF, and 15.0HF, respectively) and that of the GF was changed to 5.0, 10.0, or 15.0 mm FWHM (5.0GF, 10.0GF, and 15.0GF, respectively). We determined the effect of the filters on MBF calculation using a summed image of the early dynamic phase in the HV study. The parameters of the OSEM algorithm tested were combinations of 4S and 2I, 4I, 6I, or 8I (4S2I, 4S4I, 4S6I, or 4S8I) of 16S and 2I, 4I, 6I, or 8I (16S2I, 16S4I, 16S6I, or 16S8I) of 28S and 2I, 4I, 6I, or 8I (28S2I, 28S4I, 28S6I, or 28S8I) using the optimum size of the GF, which was applied to the patient study. The values of MBF and k_{mono}, which were calculated using each parameter of the OSEM algorithm (MBF_{OSEM} and $k_{monoOSEM}$, respectively), were compared with those calculated using the FBP algorithm (MBF_{FBP} and $k_{monoFBP}$, respectively). These PET images were corrected using radioactive decay to the start time, a deconvolution scatter correction method [24], and the recovery coefficient of the PET camera.

Quantitative analysis

The MBF (ml/min/g) values were calculated by a Patlak plot using dynamic image data reconstructed with FBP and OSEM algorithms as reported previously [12,25]. A summed image of data obtained 30–150 s after the start of PET acquisition as well as MRI T1 images were used to place regions of interest (ROIs) in a suitable position. Fifteen ROIs (5 × 3 slices) of 6.0 mm diameter were drawn in the left ventricular (LV) cavity to obtain a time–activity curve (TAC) of arterial input function [26] and in anterior (ANT), septal (SEP), inferior (INF), posterior (POS), and lateral (LAT) walls to obtain TACs of each

Fig. 1

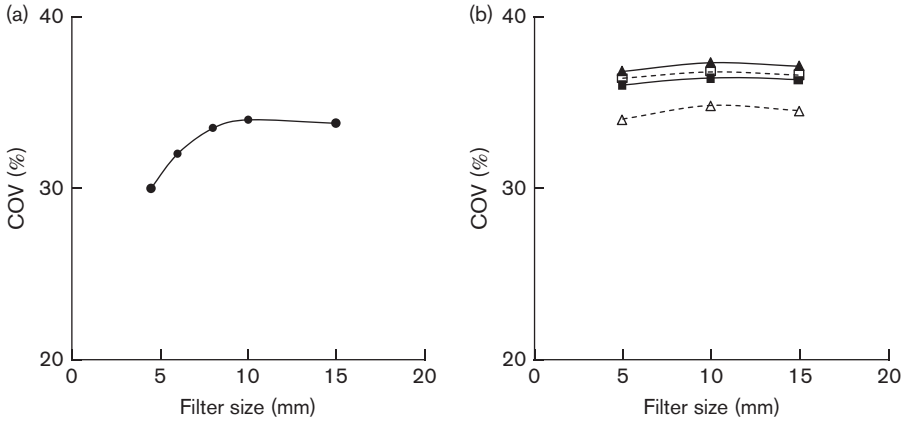

(a) Effect of smoothing filter size on filtered back-projection and ordered-subset expectation maximization algorithms at the global myocardium in healthy volunteers. The value of the coefficient of variation (COV) reached a maximum when a 10.0 mm full-width resolution at half-maximum hanning filter was applied in the filtered back-projection algorithm. (b) A filter size of 10.0 mm full-width resolution at half-maximum was best for a Gaussian post-filter in the ordered-subset expectation maximization algorithm using parameters of 28S and 2I (△), 4I (□), 6I (▲) or 8I (■).

Table 1 MBF values at the global myocardium and myocardial region in HV and CAD patients

			OSEM											
		Subset	4				16				28			
Region	FBP	Iteration	2	4	6	8	2	4	6	8	2	4	6	8
HV														
Global	0.60 ± 0.14		0.28 ± 0.08*	0.39 ± 0.12*	0.46 ± 0.10*	0.49 ± 0.10*	0.49 ± 0.09*	0.56 ± 0.10*	0.58 ± 0.11	0.60 ± 0.12	0.55 ± 0.10*	0.59 ± 0.12	0.61 ± 0.14	0.62 ± 0.14**
ANT	0.59 ± 0.12		0.26 ± 0.04*	0.38 ± 0.05*	0.44 ± 0.06*	0.47 ± 0.06*	0.47 ± 0.06*	0.53 ± 0.08**	0.56 ± 0.09	0.58 ± 0.10	0.53 ± 0.09	0.57 ± 0.10	0.59 ± 0.13	0.60 ± 0.13
SEP	0.64 ± 0.08		0.29 ± 0.17*	0.41 ± 0.18	0.46 ± 0.16	0.49 ± 0.15	0.49 ± 0.15	0.57 ± 0.11	0.61 ± 0.10	0.63 ± 0.10	0.53 ± 0.09	0.62 ± 0.10	0.64 ± 0.10	0.65 ± 0.11
INF	0.56 ± 0.18		0.29 ± 0.07*	0.43 ± 0.11*	0.48 ± 0.13**	0.51 ± 0.14	0.51 ± 0.14	0.54 ± 0.15	0.55 ± 0.16	0.56 ± 0.17	0.53 ± 0.13	0.56 ± 0.16	0.57 ± 0.18	0.57 ± 0.18
POS	0.60 ± 0.14		0.18 ± 0.08*	0.23 ± 0.08*	0.37 ± 0.06*	0.43 ± 0.06**	0.43 ± 0.05**	0.54 ± 0.08	0.57 ± 0.10	0.59 ± 0.11	0.54 ± 0.11	0.59 ± 0.12	0.61 ± 0.13	0.62 ± 0.14
LAT	0.60 ± 0.13		0.29 ± 0.06*	0.36 ± 0.13*	0.45 ± 0.08*	0.48 ± 0.08**	0.48 ± 0.08**	0.55 ± 0.08	0.57 ± 0.09	0.58 ± 0.10	0.54 ± 0.08	0.59 ± 0.10	0.60 ± 0.12	0.61 ± 0.13
CAD														
Ischemia	0.21 ± 0.09		0.12 ± 0.13	0.14 ± 0.14	0.15 ± 0.12	0.17 ± 0.11	0.17 ± 0.11	0.20 ± 0.09	0.20 ± 0.09	0.21 ± 0.09	0.19 ± 0.10	0.21 ± 0.09	0.21 ± 0.09	0.21 ± 0.09

Values are mean values ± SD.
ANT, anterior; CAD, coronary artery disease; FBP, filtered back-projection; HV, healthy volunteer; INF, inferior; LAT, lateral; MBF, myocardial blood flow; OSEM, ordered-subset expectation maximization; POS, posterior; SEP, septal.
*$P < 0.01$ and **$P < 0.05$ compared with MBF_{FBP} using analysis of variance and a post-hoc test.

myocardial region in HV and in the LV cavity and the ischemia region in the CAD patients, using dynamic image data obtained 30–150 s from the start of PET acquisition. The average MBF values of global myocardium were calculated using the values of ANT, SEP, INF, POS, and LAT.

The k_{mono} values were calculated by a graphical analysis method using dynamic image data obtained between 8 and 20 min of ^{11}C-acetate PET [22]. A summed image of data obtained over 8–20 min as well as MRI T1 images were used to place ROIs in a suitable position. Fifteen ROIs (5×3 slices) were placed over the ANT, SEP, INF, POS, and LAT regions of dynamic images of HV, and the ischemia region of the dynamic images of the CAD patients, to obtain the TAC of each myocardial region. The average k_{mono} values of global myocardium were calculated using the values of ANT, SEP, INF, POS, and LAT. The k_{mono} values were obtained using the equation $q = Ae^{-kt}$ [where q = count/pixel/ min corrected for physical decay, $k = k_{mono}$ (per min), and t = time (min)] [25,27,28]. A monoexponential function was fitted to the TAC of each myocardial region and the values of k_{mono} were determined.

Statistical analysis

Image noise was defined as the coefficient of variation [COV, SD/mean × 100 (%)] of the pixel values within the global myocardium using the HF and the GF filters in the HV study. The values for MBF_{OSEM} and $k_{monoOSEM}$ were compared with those of MBF_{FBP} and $k_{monoFBP}$ using analysis of variance and a post-hoc test. The correlation between MBF_{FBP} and MBF_{OSEM} and that between $k_{monoFBP}$ and $k_{monoOSEM}$ were evaluated using linear regression analysis. Agreements between MBF_{FBP} and MBF_{OSEM} and between $k_{monoFBP}$ and $k_{monoOSEM}$ were analyzed by Bland–Altman plots that show the differences (FBP – OSEM) versus the entire range of average values ± 2SD [29,30].

Results

Myocardial blood flow calculation

The smoothing effect of the different sizes of each filter tested using the FBP and OSEM algorithms was determined (Fig. 1). The COV reached a maximum of 32% when 10.0HF was applied to the projection data of the FBP algorithm. In the OSEM algorithm, 10.0GF yielded the maximum COV, although the COV did not change significantly when the size of the GF was changed. Conditions of 10.0HF and 10.0GF were then applied to the FBP and OSEM algorithms, respectively, to evaluate combinations of different S and I values in the OSEM algorithm. The MBF values of the global myocardium and of myocardial regions in HV, and of the ischemia region in CAD patients, were determined (Table 1). The MBF_{OSEM} that was calculated for the global myocardium of HV using 16S6I, 16S8I, 28S4I, or 28S6I was not significantly different from the MBF_{FBP} calculated for the same region. In the

Table 2 Correlation of MBF_{FBP} and MBF_{OSEM} on the global myocardium in HV and CAD patients

Subset	4				16				28			
Iteration	2	4	6	8	2	4	6	8	2	4	6	8
HV												
Slope[a]	0.15	0.45	0.46	0.53	0.52	0.69	0.79	0.88	0.66	0.85	0.97	1.02
r^2	0.07	0.27	0.42	0.57	0.58	0.86	0.93	0.94	0.87	0.93	0.96	0.96
CAD												
Slope[a]	0.42	0.43	0.53	0.62	0.62	0.83	0.97	0.98	0.78	0.93	0.99	1.02
r^2	0.08	0.08	0.14	0.22	0.23	0.59	0.83	0.90	0.48	0.85	0.93	0.95

CAD, coronary artery disease; FBP, filtered back-projection; HV, healthy volunteer; MBF, myocardial blood flow; OSEM, ordered-subset expectation maximization.
[a]Slope of the regression line between MBF_{FBP} and MBF_{OSEM}.

Fig. 2

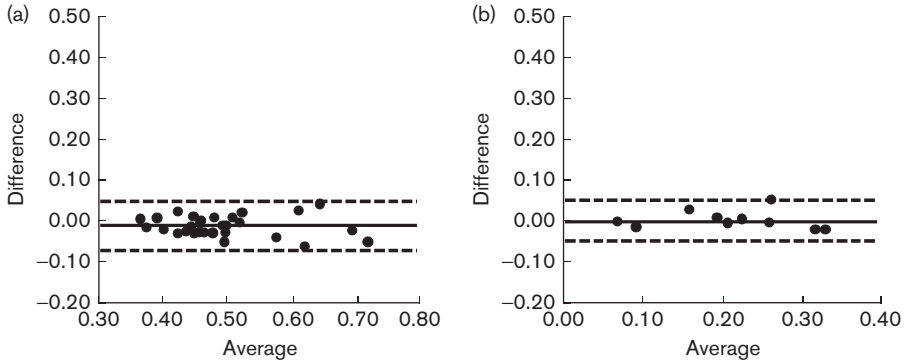

(a) Bland–Altman analyses of myocardial blood flow showing the differences between the average filtered back-projection and each parameter of ordered-subset expectation maximization in healthy volunteers and (b) in coronary artery disease patients. The magnitude of the bias was small (−0.01 ml/min/g in the HV and 0.00 ml/min/g in the coronary artery disease patients), with limits of agreement ranging from values of 0.05 ml/min/g. Means (solid lines) ± 2SD (broken line) are shown.

myocardial regions, differences between MBF_{FBP} and MBF_{OSEM}, calculated using increasing S and I numbers in the OSEM algorithm, were not significant. In the CAD patient group, there were no significant differences between the value of MBF_{FBP} and the value of MBF_{OSEM} calculated using any combination of S and I. The correlation between MBF_{FBP} and MBF_{OSEM} at the global myocardium in HV and in CAD patients was calculated (Table 2). In the correlation between MBF_{FBP} and MBF_{OSEM}, the slope of the regression line was improved by increasing the S and I numbers of the OSEM algorithm in HV and in CAD patients. The best correlations were between MBF_{FBP} and MBF_{OSEM} with 28S6I in HV and with 28S8I at the ischemia region of the CAD patients. The mean differences between MBF_{FBP} and MBF_{OSEM} with 28S6I were -0.01 ± 0.05 ml/min/g in the HV patients and 0.00 ± 0.05 ml/min/g in the CAD patients, as assessed using Bland–Altman analysis (Fig. 2).

k_{mono} calculation

The values of $k_{monoOSEM}$ that were calculated using 4S2I or 4S4I, and 10.0GF were significantly different from the value of $k_{monoFBP}$ in HV (Table 3). The slope of the regression line and the square of the correlation coefficient between $k_{monoFBP}$ and $k_{monoOSEM}$ were large, with the exception of $k_{monoOSEM}$ with 4S2I and 4S4I (Table 4). The mean differences between the value of $k_{monoFBP}$ and that of $k_{monoOSEM}$ with 28S6I, which are the optimal parameters for measurement of MBF_{OSEM}, were 0.000 ± 0.005 in HV and 0.000 ± 0.006 in the CAD patients, as assessed using Bland–Altman analysis (Fig. 3).

Discussion

The iterative reconstruction algorithm including OSEM has been improved to provide clear PET images compared with the FBP algorithm. Although some kinds of iterative reconstruction algorithms are installed in clinical PET scanners [31,32], it is difficult for technicians or operators to determine appropriate parameters of the algorithm in an effort to yield accurate quantitative PET values. This study evaluated the effects of the smoothing filter function, and the number of S and I in the OSEM algorithm, on the measurement of MBF and k_{mono} values using ^{11}C-acetate PET. The OSEM algorithm is useful for clinical PET studies because this algorithm improves image quality and reduces streak artifacts compared with the FBP algorithm [2]. Application of a smoothing filter further decreases image noise in

Table 3 k_{mono} values of the global myocardium and myocardial region in HV and CAD patients

		OSEM													
		Subset	4				16			28					
Region	FBP	Iteration	2	4	6	8	2	4	6	8	2	4	6	8
HV														
Global	0.063 ± 0.018		0.052 ± 0.013*	0.059 ± 0.016*	0.061 ± 0.016	0.062 ± 0.017	0.062 ± 0.017	0.062 ± 0.018	0.062 ± 0.018	0.062 ± 0.018	0.062 ± 0.018	0.062 ± 0.018	0.062 ± 0.018	0.062 ± 0.018
ANT	0.064 ± 0.013		0.059 ± 0.010**	0.061 ± 0.015*	0.063 ± 0.014	0.063 ± 0.014	0.063 ± 0.014	0.063 ± 0.014	0.063 ± 0.014	0.064 ± 0.013	0.063 ± 0.014	0.063 ± 0.014	0.063 ± 0.014	0.063 ± 0.014
SEP	0.067 ± 0.019		0.054 ± 0.013**	0.063 ± 0.017	0.066 ± 0.016	0.069 ± 0.019	0.069 ± 0.019	0.070 ± 0.022	0.070 ± 0.022	0.069 ± 0.022	0.070 ± 0.022	0.069 ± 0.022	0.070 ± 0.021	0.070 ± 0.021
INF	0.063 ± 0.017		0.050 ± 0.008**	0.054 ± 0.012**	0.060 ± 0.014	0.060 ± 0.014	0.060 ± 0.014	0.060 ± 0.014	0.061 ± 0.016	0.061 ± 0.016	0.060 ± 0.014	0.060 ± 0.014	0.060 ± 0.016	0.064 ± 0.016
POS	0.060 ± 0.020		0.050 ± 0.015**	0.056 ± 0.016	0.059 ± 0.019	0.059 ± 0.019	0.060 ± 0.019	0.061 ± 0.020	0.060 ± 0.020	0.059 ± 0.017	0.061 ± 0.019	0.060 ± 0.017	0.057 ± 0.019	0.057 ± 0.019
LAT	0.060 ± 0.017		0.053 ± 0.016*	0.060 ± 0.019	0.059 ± 0.018	0.059 ± 0.018	0.059 ± 0.018	0.060 ± 0.017	0.059 ± 0.019	0.059 ± 0.018	0.059 ± 0.019	0.057 ± 0.019	0.057 ± 0.019	0.059 ± 0.018
CAD														
Ischemia	0.027 ± 0.014		0.030 ± 0.011	0.031 ± 0.012	0.030 ± 0.013	0.029 ± 0.013	0.028 ± 0.013	0.027 ± 0.015	0.026 ± 0.016	0.026 ± 0.016	0.028 ± 0.015	0.027 ± 0.016	0.027 ± 0.016	0.027 ± 0.016

Values are mean values ± SD.
ANT, anterior; CAD, coronary artery disease; FBP, filtered back-projection; HV, healthy volunteer; INF, inferior; LAT, lateral; OSEM, ordered-subset expectation maximization; POS, posterior; SEP, septal.
*P < 0.01 and **P < 0.05 compared with MBF_{FBP} using analysis of variance and a post-hoc test.

PET images. In this study, the effect of the smoothing filter on MBF calculation was evaluated using early time frames with a short time duration, because the images in the frame have considerable image noise. The GF in the OSEM algorithm was optimized at 10.0 mm FWHM, at which point the maximum COV of 35–40% was attained. This maximum was higher than that obtained with the FBP algorithm after optimization of the HF in the FBP algorithm (Fig. 1). Therefore, the image quality using OSEM is greater than that using FBP, which produces considerable image noise. The MBF_{FBP} using 10.0HF was 0.60 ± 0.14 ml/min/g at the global myocardium in HV. In a previous study, MBF_{FBP} calculated using a Shepp filter of Nyquist frequency (0.3 cycles per pixel) was 0.70 ± 0.11 ml/min/g in HV using ^{11}C-acetate [20]. Although this Shepp filter was not optimized for the measurement of MBF_{FBP} with ^{11}C-acetate, no significant differences were observed between the MBF_{FBP} that was calculated using the Shepp filter and that calculated using the HF. Kudo *et al.* [12] showed that the MBF_{FBP} values calculated for ^{11}C-acetate showed an excellent linear correlation with those calculated for ^{13}N-ammonia using a Patlak plot. In ^{11}C-acetate PET, the values of MBF_{OSEM} were close to those of MBF_{FBP} at the global myocardium and at each myocardial region when the number of S and I were increased, especially in HV (Table 1). The best correlations were between the value of MBF_{FBP} with 10.0HF and that of MBF_{OSEM} with 28S6I and 10.0GF at the global myocardium of HV or that of MBF_{OSEM} with 28S8I and 10.0GF at the ischemia region of the CAD patients (Table 2). However, the MBF_{OSEM} with 28S8I was significantly different from the MBF_{FBP} at the global myocardium in HV because image noise was elevated with increasing iteration in the OSEM algorithm. As a result, the COV of 28S8I was slightly smaller than that of 28S6I (Fig. 1). Thus, high iteration numbers should not be used in the OSEM algorithm for quantitative PET studies. There was excellent agreement between the value of the average MBF of each participant, calculated using MBF_{OSEM} with 28S6I and 10.0GF, and MBF_{FBP} with 10.0HF in HV and CAD patients (Fig. 2). The short-axis MBF_{OSEM} images obtained using 28S6I and 10.0GF were clear compared with MBF_{FBP} images obtained with 10.0HF (Figs 4 and 5). Therefore, when using ^{11}C-acetate PET, parameters of 28S6I and 10.0GF should be used for the measurement of MBF_{OSEM}. The excellent quality of the MBF_{OSEM} images will improve diagnostic performance in PET studies. For example, misregistration between transmission attenuation and emission images causes artifactual abnormalities on cardiac PET images that result in false-positive defects [33,34]. The severe artifacts are produced by diaphragmatic displacement, BMI, and heart sizes. These artifacts can be decreased using the appropriate parameter of the OSEM algorithm.

The MBF_{OSEM} values were compared with the MBF_{FBP} values of previous cardiac ^{15}N-ammonia PET studies [4–6].

Table 4 Correlation of $k_{monoFBP}$ and $k_{monoOSEM}$ on the global myocardium in HV and CAD patients

Subset	4				16				28			
Iteration	2	4	6	8	2	4	6	8	2	4	6	8
HV												
Slope[a]	0.69	0.84	0.90	0.94	0.94	1.00	1.01	0.99	1.00	1.01	1.01	1.01
r^2	0.87	0.90	0.96	0.97	0.97	0.98	0.98	0.98	0.97	0.97	0.96	0.95
CAD												
Slope[a]	0.56	0.66	0.75	0.82	0.84	1.00	1.07	1.10	0.99	1.10	1.11	1.08
r^2	0.50	0.62	0.75	0.84	0.82	0.96	0.98	0.98	0.95	0.98	0.97	0.95

CAD, coronary artery disease; FBP, filtered back-projection; HV, healthy volunteer; MBF, myocardial blood flow; OSEM, ordered-subset expectation maximization.
[a]Slope of the regression line between MBF_{FBP} and MBF_{OSEM}.

Fig. 3

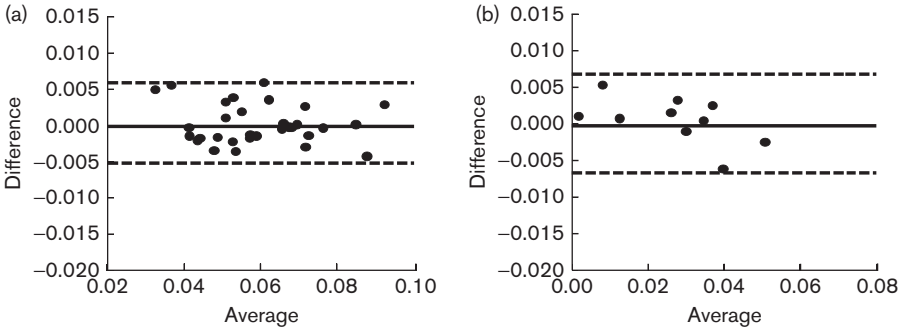

Bland–Altman analyses of k_{mono} showing the differences between the average filtered back-projection and each parameter of ordered-subset expectation maximization in healthy volunteers (a) and coronary artery disease patients (b). There was no difference between $k_{monoFBP}$ and $k_{monoOSEM}$. Means (solid lines) ± 2SD (broken line) are shown.

Søndergaard *et al.* [4] showed the usefulness of OSEM with 16S6I and 8.0GF compared with FBP and a ramp filter. However, as they did not perform partial volume correction in that study, the MBF values calculated using these parameters of the OSEM algorithm will not be accurate. Chen *et al.* [5] assessed the effects of changing the number of I and the smoothing filter of the OSEM algorithm on MBF. In their study, the value of MBF_{OSEM} with 28S8I and 10.0GF correlated best with MBF_{FBP} with 10.0HF. However, the parameters of the OSEM algorithm were not optimized in that study, because they did not assess the effect of combinations of S and I numbers. Hove *et al.* [6] estimated MBF_{OSEM} values using 28S2I and 6.0HF, which is the default setting of the equipment. They reported that this value was underestimated compared with the value obtained using MBF_{FBP} and 7.0 mm FWHM HF or with the value obtained by Chen *et al*. When appropriate parameters (16S4I or 16S6I) of the OSEM algorithm were applied, the OSEM algorithm was also shown to be a useful tool in previous cardiac ^{18}F-FDG PET studies for improving image quality [2–4]. Although these reported parameters for the OSEM algorithm in ^{15}N-ammonia and ^{18}F-FDG studies are not significantly different from the 28S6I with 10.0GF parameters, which were appropriate for MBF evaluation using ^{11}C-acetate PET in our study, none of these previous studies ever evaluated in detail the effect of combinations of S and I numbers and different filter sizes on MBF measurement.

Using ^{11}C-acetate PET, it is possible to easily measure not only the MBF value [7–12] but also the k_{mono} values [13–22]. The present study is the first to investigate the effect of parameters of OSEM algorithms on the measurement of k_{mono} using a graphical analysis method of monoexponential curve fitting and data obtained 8–20 min after ^{11}C-acetate injection [22]. Filter sizes of 10.0HF and 10.0GF, which are appropriate for the measurement of MBF, were applied to k_{mono} measurement because smoothing filters had a greater effect on MBF measurement than on k_{mono} measurement. The $k_{monoOSEM}$ values obtained were not significantly different from the $k_{monoFBP}$ values, with the exception of values obtained using 4S2I and 4S4I in HV (Table 3). The effect of increasing S and I on the measurement of k_{mono} would be small. Bland–Altman analysis indicated no difference between the value of $k_{monoOSEM}$ obtained using 28S6I and 10.0GF and $k_{monoFBP}$ with 10.0HF (Fig. 3). The OSEM algorithm with 28S6I and 10.0GF produced clear $k_{monoOSEM}$ images compared with $k_{monoFBP}$ with 10.0HF (Figs 4 and 5). Therefore, parameters of 28S6I and 10.0GF in the OSEM algorithm are appropriate for

Fig. 4

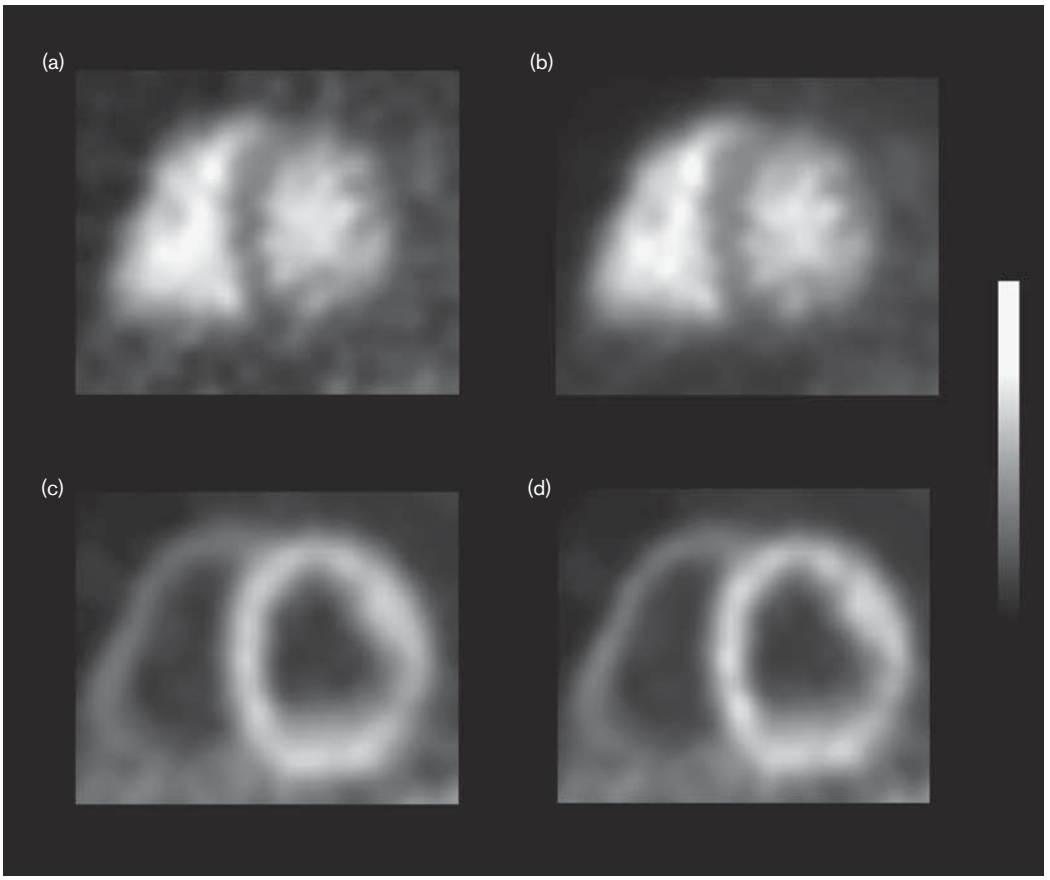

Representative short-axis images for the calculation of (a) MBF_{FBP}, (b) MBF_{OSEM}, (c) $k_{monoFBP}$, and (d) $k_{monoOSEM}$ in HV. The MBF values were calculated based on Patlak-plot analyses using early-phase dynamic images. These images were summed using early-phase dynamic data for the calculation of MBF and later-phase data obtained 8–20 min after ^{11}C-acetate injection for the calculation of k_{mono}. FBP, filtered back-projection; MBF, myocardial blood flow; OSEM, ordered-subset expectation maximization.

calculation of the MBF_{OSEM} and $k_{monoOSEM}$ values in ^{11}C-acetate PET. The reconstruction time using adequate parameters of the OSEM algorithm was little different from that with the FBP algorithm due to recent progress in computer performance. It will be possible to apply these 28S6I with 10.0GF parameters that were appropriate in ^{11}C-acetate PET for the measurement of MBF_{OSEM} using ^{15}N-ammonia PET because both ^{11}C-acetate and ^{15}N-ammonia can measure the MBF of myocardium.

The appropriate parameters of the OSEM algorithm defined in this study will be applicable to other 2D-PET scanners if a radiotracer with a similar level of radioactivity is injected, because the total counts are generally determined by injection radioactivity in 2D-PET scanners. The intrinsic spatial resolution of the PET scanner will not be related to measurement of MBF and k_{mono} because the sizes of the ROIs that are drawn over the LV cavity and the myocardial region are larger than the spatial resolution, and PET counts in the ROI are sufficient for calculation of the MBF and k_{mono}. However, the parameters defined in this study could not be applied to three-dimensional (3D)-PET because, even with the same injected radioactivity for a 2D-PET and a 3D-PET scan, the total counts of 3D-PET, including several scatter counts, will increase compared with those of 2D-PET with a septa system. In addition, the appropriate parameters cannot be used in the OSEM algorithm when the detectable level of radioactive counts increases significantly on a PET scanner with a new detector and acquisition technology compared with conventional PET scanners. We have not attempted to determine the effect of a loop filter in the OSEM algorithm in the General Electric Medical System scanner because smoothing GF strength is an essential factor for the reduction of image noise in PET images in other scanners. If analysis of other detailed parameters of the OSEM algorithm are required, such a study would necessitate a much larger population of patients as well as evaluation of diagnostic performance.

Fig. 5

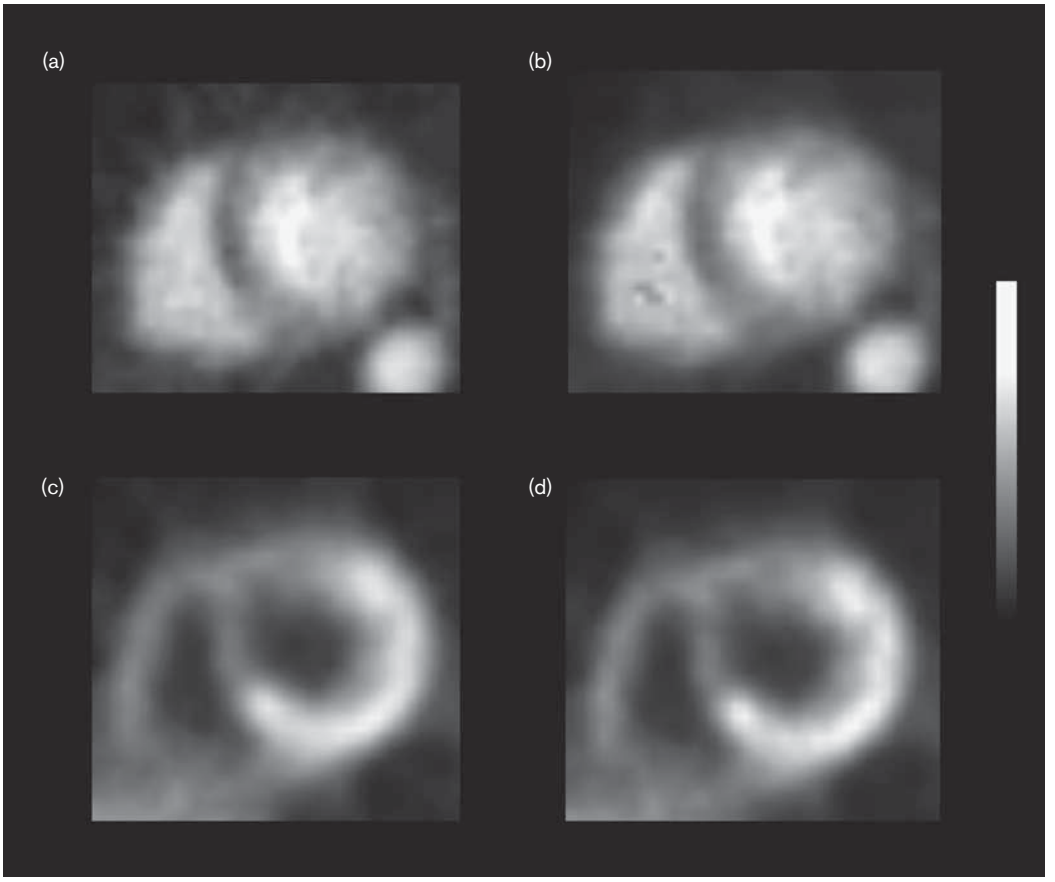

Representative short-axis images for the calculation of (a) MBF_{FBP}, (b) MBF_{OSEM}, (c) $k_{monoFBP}$, and (d) $k_{monoOSEM}$ in coronary artery disease patients with ischemia of ANT and SEP walls. These images were summed using early-phase dynamic data for the calculation of MBF and later-phase data obtained 8–20 min after ^{11}C-acetate injection for the calculation of k_{mono}. FBP, filtered back-projection; MBF, myocardial blood flow; OSEM, ordered-subset expectation maximization.

Conclusion

Application of the OSEM algorithm to a PET study yields noiseless, artifact-reduction images and quantitative PET values when the smoothing filter size and the numbers of S and I are optimized. Parameters of OSEM that are adequate for the measurement of MBF_{OSEM} and $k_{monoOSEM}$ using ^{11}C-acetate PET are 28S6I with a 10.0GF.

Acknowledgements

The authors thank Satonao Nakakoji, Akira Ito, Hiroshi Oikawa, and other staff of the Biological Imaging Research Center, the University of Fukui, for their technical support.

This study was partly funded by Grants-in-Aid for Scientific Research from Japan Society for the Promotion of Science (19790862, 20249055, 21390342, 21591551, 21659286, 22659219, 22791180, and 23300361) and the Fukui Brain Project, Research and Education Program for Life Science, University of Fukui.

Conflicts of interest

There are no conflicts of interest.

References

1 Hudson HM, Larkin RS. Accelerated image-reconstruction using ordered subsets of projection data. *IEEE Trans Med Imaging* 1994; **13**:601–609.
2 Boellaard R, van Lingen A, Lammertsma AA. Experimental and clinical evaluation of iterative reconstruction (OSEM) in dynamic PET: quantitative characteristics and effects on kinetic modeling. *J Nucl Med* 2001; **42**: 808–817.
3 Lubberink M, Boellaard R, van der Weerdt AP, Visser FC, Lammertsma AA. Quantitative comparison of analytic and iterative reconstruction methods in 2- and 3-dimensional dynamic cardiac ^{18}F-FDG PET. *J Nucl Med* 2004; **45**:2008–2015.
4 Søndergaard HM, Madsen MM, Boisen K, Bøttcher M, Schmitz O, Nielsen TT, *et al*. Evaluation of iterative reconstruction (OSEM) versus filtered back-projection for the assessment of myocardial glucose uptake and myocardial perfusion using dynamic PET. *Eur J Nucl Med Mol Imaging* 2007; **34**:320–329.
5 Chen GP, Branch KR, Alessio AM, Pham P, Tabibiazar R, Kinahan P, *et al*. Effect of reconstruction algorithms on myocardial blood flow measurement with ^{13}N-ammonia PET. *J Nucl Med* 2007; **48**:1259–1265.

6 Hove JD, Rasmussen R, Freiberg J, Holm S, Kelbaek H, Kofoed KE. Clinical evaluation of iterative reconstruction (ordered-subset expectation maximization) in dynamic positron emission tomography: quantitative effects on kinetic modeling with N-13 ammonia in healthy subjects. *J Nucl Cardiol* 2008; **15**:530–534.

7 Gropler RJ, Siegel BA, Geltman EM. Myocardial uptake of carbon-11-acetate as an indirect estimate of regional myocardial blood flow. *J Nucl Med* 1991; **32**:245–251.

8 Van den Hoff J, Burchert W, Wolpers HG, Meyer GJ, Hundeshagen H. A kinetic model for cardiac PET with [1-carbon-11]-acetate. *J Nucl Med* 1996; **37**:521–529.

9 Sun KT, Yeatman LA, Buxton DB, Chen K, Johnson JA, Huang SC, *et al*. Simultaneous measurement of myocardial oxygen consumption and blood flow using [1-carbon-11]acetate. *J Nucl Med* 1998; **39**:272–280.

10 Sciacca RR, Akinboboye O, Chou RL, Epstein S, Bergmann SR. Measurement of myocardial blood flow with PET using 1-^{11}C-acetate. *J Nucl Med* 2001; **42**:63–70.

11 van den Hoff J, Burchert W, Börner AR, Fricke H, Kühnel G, Meyer GJ, *et al*. [1-carbon-11]-Acetate as a quantitative perfusion tracer in myocardial PET. *J Nucl Med* 2001; **42**:1174–1182.

12 Kudo T, Hata T, Kagawa S, Kishibe Y, Iwasaki J, Nakano A, *et al*. Simple quantification of myocardial perfusion by pixel-by-pixel graphical analysis using carbon-11 acetate: comparison of the K-complexes of carbon-11 acetate and nitrogen-13 ammonia. *Nucl Med Commun* 2008; **29**:679–685.

13 Brown M, Marshall DR, Sobel BE, Bergmann SR. Delineation of myocardial oxygen utilization with carbon-11-labeled acetate. *Circulation* 1987; **76**:697–696.

14 Brown MA, Myears DW, Bergmann SR. Noninvasive assessment of canine myocardial oxidative metabolism with carbon-11 acetate and positron emission tomography. *J Am Coll Cardiol* 1988; **12**:1054–1063.

15 Brown MA, Myears DW, Bergmann SR. Validity of estimates of myocardial oxidative metabolism with carbon-11 acetate and positron emission tomography despite altered patterns of substrate utilization. *J Nucl Med* 1989; **30**:187–193.

16 Buxton DB, Nienaber CA, Luxen A, Ratib O, Hansen H, Phelps ME, *et al*. Noninvasive quantitation of regional myocardial oxygen consumption in vivo with [1-^{11}C]acetate and dynamic positron emission tomography. *Circulation* 1989; **79**:134–142.

17 Henes CG, Bergmann SR, Walsh MN, Sobel BE, Geltman EM. Assessment of myocardial oxidative metabolic reserve with positron emission tomography and carbon-11 acetate. *J Nucl Med* 1989; **30**:1489–1499.

18 Armbrecht JJ, Buxton DB, Brunken RC, Phelps ME, Schelbert HR. Regional myocardial oxygen consumption determined noninvasively in humans with [1-^{11}C]acetate and dynamic positron tomography. *Circulation* 1989; **80**:863–872.

19 Armbrecht JJ, Buxton DB, Brunken RC, Phelps ME, Schelbert HR. Validation of [1-^{11}C]acetate as a tracer for noninvasive assessment of oxidative metabolism with positron emission tomography in normal, ischemic, postischemic, and hyperemic canine myocardium. *Circulation* 1990; **81**:1594–1605.

20 Sun KT, Chen K, Huang SC, Buxton DB, Hansen HW, Kim AS, *et al*. Compartment model for measuring myocardial oxygen consumption using [1-^{11}C]acetate. *J Nucl Med* 1997; **38**:459–466.

21 Klein LJ, Visser FC, Knaapen P, Peters JH, Teule GJ, Visser CA, *et al*. Carbon-11 acetate as a tracer of myocardial oxygen consumption. *Eur J Nucl Med* 2001; **28**:651–668.

22 Hussain R, Kudo T, Tsujikawa T, Kobayashi M, Fujibayashi Y, Okazawa H. Validation of the calculation of the clearance rate constant (k_{mono}) of [^{11}C]acetate using parametric k_{mono} image for myocardial oxidative metabolism. *Nucl Med Biol* 2009; **36**:877–882.

23 DeGrado TR, Turkington TG, Williams JJ, Stearns CW, Hoffman JM, Coleman RE. Performance characteristics of a whole-body PET scanner. *J Nucl Med* 1994; **35**:1398–1406.

24 Bergström M, Eriksson L, Bohm C, Blomqvist G, Litton J. Correction for scattered radiation in a ring detector positron camera by integral transformation of the projections. *J Comput Assist Tomogr* 1983; **7**:42–50.

25 Patlak CS, Blasberg RG, Fenstermacher JD. Graphical evaluation of blood-to-brain transfer constants from multiple-time uptake data. *J Cereb Blood Flow Metab* 1983; **3**:1–7.

26 van der Weerdt AP, Klein LJ, Boellaard R, Visser CA, Visser FC, Lammertsma AA. Image-derived input functions for determination of MRGlu in cardiac ^{18}F-FDG PET scans. *J Nucl Med* 2001; **42**:1622–1629.

27 Choi Y, Huang SC, Hawkins RA, Kuhle WG, Dahlbom M, Hoh CK, *et al*. A simplified method for quantification of myocardial blood flow using nitrogen-13-ammonia and dynamic PET. *J Nucl Med* 1993; **34**:488–497.

28 Choi Y, Huang SC, Hawkins RA, Kim JY, Kim BT, Hoh CK, *et al*. Quantification of myocardial blood flow using 13N-ammonia and PET: comparison of tracer models. *J Nucl Med* 1999; **40**:1045–1055.

29 Bland JM, Altman DG. Statistical methods for assessing agreement between two methods of clinical measurement. *Lancet* 1986; **1**:307–310.

30 Bland JM, Altman DG. Measuring agreement in method comparison studies. *Stat Methods Med Res* 1999; **8**:135–160.

31 Ibaraki M, Sato K, Mizuta T, Kitamura K, Miura S, Sugawara S, *et al*. Evaluation of dynamic row-action maximum likelihood algorithm reconstruction for quantitative ^{15}O brain PET. *Ann Nucl Med* 2009; **23**:627–638.

32 Inoue K, Moriya E, Suzuki T, Ohnuki Y, Sato T, Kitamura H, *et al*. The usefulness of fully three-dimensional OSEM algorithm on lymph node metastases from lung cancer with ^{18}F-FDG PET/CT. *Ann Nucl Med* 2011; **25**:277–287.

33 Loghin C, Sdringola S, Gould KL. Common artifacts in PET myocardial perfusion images due to attenuation-emission misregistration: clinical significance, causes, and solutions. *J Nucl Med* 2004; **45**:1029–1039.

34 McQuaid SJ, Hutton BF. Sources of attenuation-correction artefacts in cardiac PET/CT and SPECT/CT. *Eur J Nucl Med Mol Imaging* 2008; **35**:1117–1123.